iScience

Article

A lysosome-targeted fluorescent probe with large Stokes shift for visualizing biothiols *in vivo* and *in vitro*

Graphical abstract

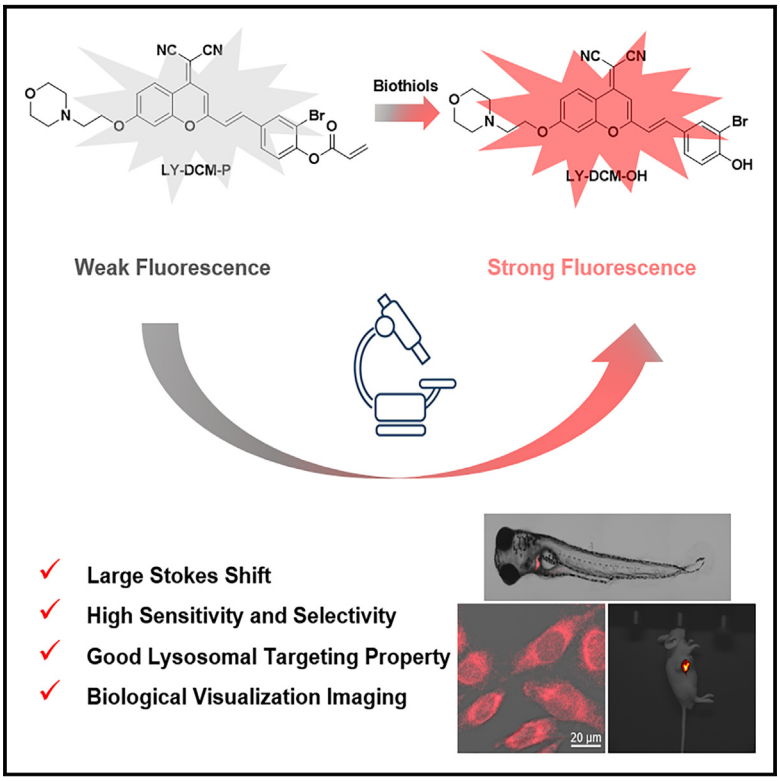

Authors

Taotao Zhao, Tong Zhang, Zijun Tao, ..., Feiyi Wang, Jun Ren, Erfei Wang

Correspondence

wuzj@hubu.edu.cn (Z.W.),
renjun@hubu.edu.cn (J.R.),
efwang@hubu.edu.cn (E.W.)

In brief

Chemistry; Physics; Biological sciences

Highlights

- A lysosome-targeted fluorescent probe LY-DCM-P was constructed to detect biothiols
- LY-DCM-P exhibits red fluorescence (670 nm) upon binding to biological thiols
- LY-DCM-P can be used for rapid and highly selective detection of biological thiols
- LY-DCM-P has effectively monitored the endogenous biothiols in living systems

Zhao et al., 2024, iScience *27*, 111334
December 20, 2024
https://doi.org/10.1016/j.isci.2024.111334

CellPress

iScience

CellPress
OPEN ACCESS

Article

A lysosome-targeted fluorescent probe with large Stokes shift for visualizing biothiols *in vivo* and *in vitro*

Taotao Zhao,[1,2] Tong Zhang,[1,2] Zijun Tao,[1] Zhe Zhou,[1] Xiaofeng Xia,[1] Zhengjun Wu,[1,*] Feiyi Wang,[1] Jun Ren,[1,*] and Erfei Wang[1,3,*]

[1]Hubei Key Laboratory for Precision Synthesis of Small Molecule Pharmaceuticals & Ministry of Education Key Laboratory for the Synthesis and Application of Organic Functional Molecules, Hubei University, Wuhan 430062, P.R. China

[2]These authors contributed equally

[3]Lead contact

*Correspondence: wuzj@hubu.edu.cn (Z.W.), renjun@hubu.edu.cn (J.R.), efwang@hubu.edu.cn (E.W.)

https://doi.org/10.1016/j.isci.2024.111334

SUMMARY

Lysosomal biothiols play critical roles in numerous cellular processes and diseases. Researching an effective method for real-time labeling biothiols in lysosomes is of great significance and urgency, as it could provide essential information for the diagnosis of relevant diseases. In this study, we developed a lysosome-targeted fluorescent probe (LY-DCM-P) with a large Stokes shift of 150 nm for the sensitive and selective detection of biothiols *in vivo* and *in vitro*. Additionally, LY-DCM-P showed low cytotoxicity and excellent lysosome-targeted ability. The probe was successfully employed to monitor fluctuations in lysosomal biothiols in various living systems, enabling enormous potential to accurately monitor the occurrence and progress of biothiol-related diseases.

INTRODUCTION

Biothiols, including cysteine (Cys), homocysteine (Hcy), and glutathione (GSH), are the most abundant low molecular weight active cellular thiols in organisms, playing crucial roles in alleviating the damage caused by free radicals to biological systems and maintaining the oxidative-reductive balance within the body.[1–4] Studies have shown that abnormal levels of biological thiols are associated with the development of certain diseases.[5–7] For instance, the deficiency of Cys can lead to various syndromes such as slow growth, weakness, muscle and fat loss, liver and skin damage, edema, and drowsiness.[8–10] Hcy is a non-protein amino acid that serves as an indicator for various diseases like cardiovascular diseases, osteoporosis, and neurological disorders.[11–13] GSH acts as an antioxidant, protecting cells from damage by reactive oxygen species that are linked to conditions like Aids, cancer, aging, stroke, leukopenia, and heart issues.[14–16] Therefore, researching effective methods for monitoring biological thiol levels is of great significance and urgency, as it could provide essential information for the diagnosis of relevant diseases.[17–19]

Lysosomes are vital subcellular organelles capable of degrading intracellular and extracellular substances through various internal pathways, playing critical roles in cellular digestion, immune responses, membrane repair, and energy metabolism.[20–22] Within lysosomes, biothiols are closely associated with protein hydrolysis, participating in protein breakdown by reducing disulfide bonds, primarily derived from the abundant conversion of cysteine in lysosomes.[23–25] Therefore, labeling biothiols in lysosomes is crucial for understanding the physiological roles and accurate diagnosis of lysosome-related diseases in biological systems.[26–30] Fluorescent probe technology has become a recent research focus due to its simplicity, high sensitivity, non-destructiveness.[31–35] However, many reported biothiol probes face challenges such as short emission wavelengths (<600 nm), small Stokes shifts (<100 nm), and imprecise subcellular localization.[36,37] Resolving these issues can enhance the development potential of fluorescent probes in biological detection.[38–40]

Thus, we utilized dicyanobenzothiophene as the fluorescent group, morpholine as the lysosome-targeting moiety, acrylate as the biothiol recognition group to construct a fluorescent probe named LY-DCM-P with long-wavelength emission (670 nm) and a large Stokes shift (150 nm). Due to the electron-withdrawing effect of the acrylate, LY-DCM-P exhibits low fluorescence, but upon the addition of Cys/Hcy/GSH, significant fluorescence emission can be detected at 670 nm. We studied the spectral response of the probe LY-DCM-P and further conducted research in live cancer cells and animal models. The results indicate that this fluorescent probe demonstrates high sensitivity and selectivity toward biothiols, possesses excellent lysosome-targeting capability, and can be applied for *in vivo* bioimaging.

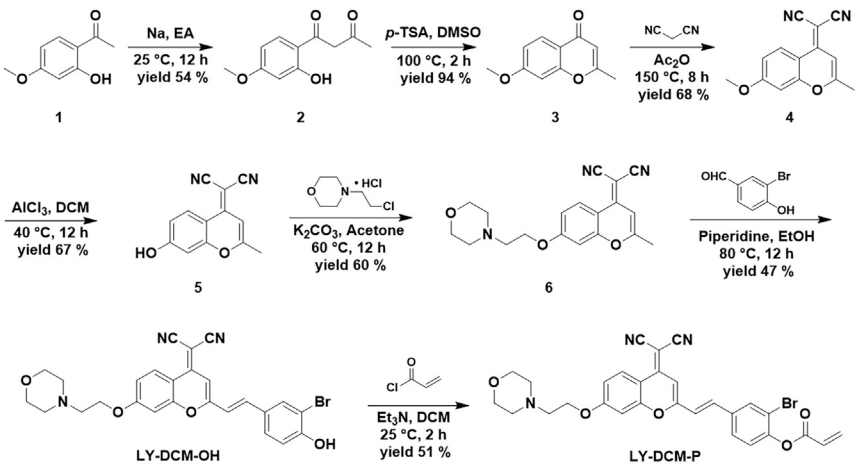

Scheme 1. The synthetic route of probe LY-DCM-P

RESULTS AND DISCUSSION

Design and synthesis of probe LY-DCM-P

As shown in Scheme 1, the synthesis steps of probe LY-DCM-P involve a series of reactions starting with the Claisen condensation, cyclization, addition, demethylation, and substitution of paeonol to obtain a compound 6 with lysosomal targeting effect. Subsequently, a Knoevenagel condensation reaction between compound 6 and 3-bromo-4-hydroxybenzaldehyde in the presence of pyridine yields the fluorescent group LY-DCM-OH. Then, under basic conditions using triethylamine, LY-DCM-OH reacts with acryloyl chloride in anhydrous dichloromethane to produce LY-DCM-P. The chemical structure was confirmed by nuclear magnetic resonance (NMR) and high-resolution mass spectrometry (HRMS) analysis (see supplemental information for details).

Spectral response of LY-DCM-P to biothiols

Firstly, the stability of probe LY-DCM-P was tested as shown in Figure S2. After a 12-h test at a constant temperature of 37°C, there was no significant change in the fluorescence intensity of the probe, demonstrating its excellent stability. Subsequently, to further explore the performance of probe LY-DCM-P, a systematic study of LY-DCM-P in the presence of different biological thiols (Cys, Hcy, and GSH) was conducted in a buffered solution at 37°C (PBS/DMSO = 3:2, 10 mM, pH = 7.4). As shown in Figures 1A–1C, the ultraviolet-visible (UV-vis) absorption spectra revealed a significant absorption enhancement at 520 nm for probe LY-DCM-P (10 μM) after interaction with Cys (40 μM)/Hcy (60 μM)/GSH (80 μM). Also, the fluorescence emission spectra of these three reaction systems all exhibited significant fluorescence enhancement at 670 nm (Figures 1D–1F). With increasing concentrations of biological thiols, the fluorescence intensity at 670 nm gradually increased, showing a good linear relationship (Figures 1G–1I). Based on these data, the detection limits (DL = 3σ/slope) of Cys/Hcy/GSH were calculated to be 42.9 nM, 75.3 nM, and 140.4 nM, respectively.

To further validate the response rates of probe LY-DCM-P to Cys, Hcy, and GSH, time course studies were also conducted. As shown in Figures 1J–1L, the graphs indicate that the three thiols reach a plateau at 10 min, 25 min, and 50 min, respectively, confirming that Cys has the fastest response rate, followed by Hcy, and then GSH. Additionally, the pH effect of LY-DCM-P was investigated, showing good stability and sensitivity to thiols across a wide pH range (Figure S3).

The selectivity of LY-DCM-P for biothiols

The selectivity of LY-DCM-P in various analytes was subsequently evaluated due to the potential need for probes to be used in complex environments. As illustrated in Figure 2, incubation of the probe with relevant active substances, such as amino acids and enzymes (Apr, aminopeptidase; Arg, arginase; Sul, sulfatase; Thr, threonine; Tyr, tyrosinase; Lip, lipase,;Ser, serine; Leu, leucine; Glu, glutamate) as well as various ions and reactive molecules (Ca^{2+}, Cu^{2+}, Fe^{2+}, Mg^{2+}, NH_4^+, NO_2^-, $S_2O_4^{2-}$, SO_4^{2-}, SO_3^{2-}, HNO, Br^-, HSO_3^-, H_2O_2, ClO^-, and HS^-), revealed subtle fluorescence changes, while the addition of Cys/Hcy/GSH resulted in a pronounced fluorescence signal. These optical responses indicate the excellent selectivity of LY-DCM-P and its potential for application in biological systems.

Sensing mechanism

The probe LY-DCM-P undergoes a nucleophilic reaction with the thiol groups in Cys/Hcy/GSH when responding to biological thiols, where the acrylate group of the probe molecule reacts with the thiol groups, causing the acrylate group to depart and resulting in the release of the fluorescent group LY-DCM-OH. To validate the reliability of the experimental design, we conducted a verification of the reaction mechanism. Initially, as shown in Figures S4A–S4C, the reaction solutions of probe LY-DCM-P with Cys/Hcy/GSH were subjected to HRMS testing, revealing the presence of the fluorescent molecule LY-DCM-OH in all three reaction solutions. Additionally, as depicted in Figures S4D–S4F, further validation of the reaction mechanism was carried out using high-performance liquid chromatography (HPLC). The retention times for probe LY-DCM-P and fluorophore LY-DCM-OH were 7.13 min and 6.07 min, respectively. Following the interaction of probe LY-DCM-P with Cys/Hcy/GSH, the retention times were in accordance with that of fluorophore LY-DCM-OH, successfully demonstrating the response mechanism of probe LY-DCM-P to biological thiols.

Cell imaging

The probe demonstrated excellent performance *in vitro*, prompting a series of biological experiments to validate its *in-vivo* applicability. Initially, the cytotoxicity of LY-DCM-P was assessed using the standard CCK-8 assay (Figure S5). Following exposure of HeLa cells and 4T1 cells to varying concentrations of LY-DCM-P

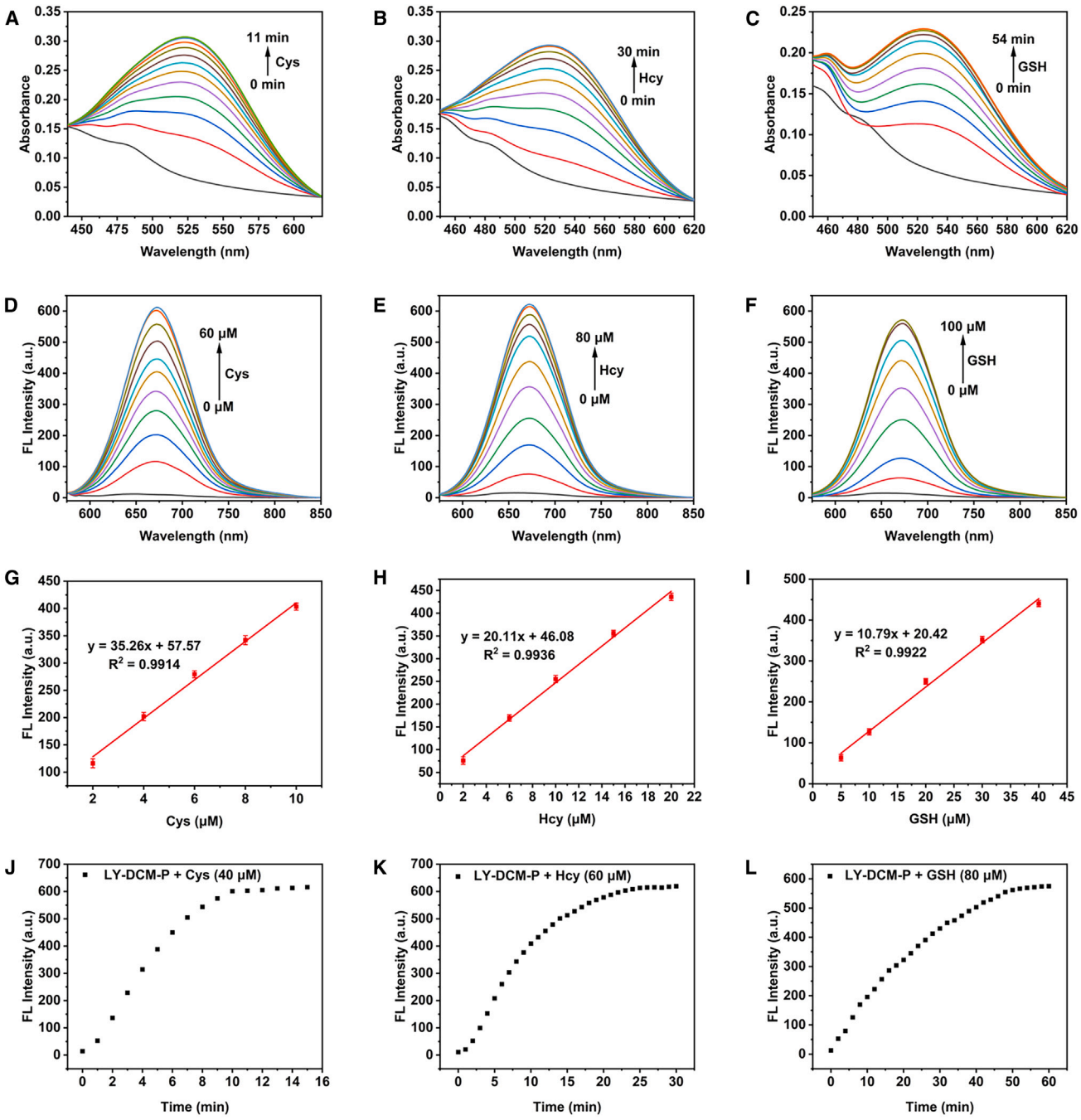

Figure 1. Spectral response results of LY-DCM-P to biothiols

(A–C) UV-vis absorption spectra of LY-DCM-P (10 μM) with Cys (40 μM)/Hcy (60 μM)/GSH (80 μM) in DMSO/PBS buffer (10 mM, 3:7, v/v, pH 7.4) at 37°C.

(D–F) Fluorescence spectra of probe LY-DCM-P (10 μM) to different concentrations of Cys/Hcy/GSH in PBS/DMSO buffer (10 mM, 3:2, v/v, pH 7.4) at 37°C, λ_{ex} = 520 nm.

(G–I) Linearity of fluorescence intensity with Cys/Hcy/GSH concentration. Data represent mean standard error (n = 3).

(J–L) Time-dependent fluorescence spectra of LY-DCM-P (10 μM) in the presence of Cys (40 μM)/Hcy (60 μM)/GSH (80 μM) in PBS/DMSO buffer (10 mM, 3:2, v/v, pH 7.4) at 37°C, λ_{ex} = 520 nm.

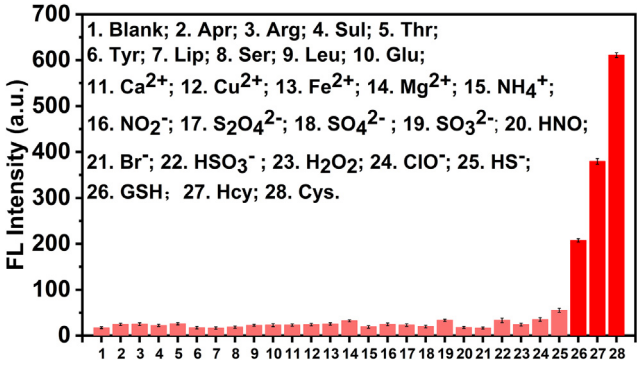

Figure 2. The selectivity results of LY-DCM-P for biothiols

Fluorescence intensity of LY-DCM-P (10 μM) after 10 min incubation with various analytes (100 μM) and Cys (40 μM)/Hcy (60 μM)/GSH (80 μM) in PBS/DMSO buffer (10 mM, 3:2, v/v, pH 7.4) at 37°C, λ_{ex} = 520 nm. Data represent mean standard error (n = 3).

(0–50 μM) for 24 h, cell viability remained above 85%, indicating low cytotoxicity toward viable cells and suitability for biological applications.

In the context of cellular imaging, the experiment involved two types of cells, HeLa cells and 4T1 cells. As depicted in the Figure 3, the HeLa cells and 4T1 cells were divided into six groups and subjected to confocal imaging experiments systematically. Compared with the control group (Figures 3A1–A6), fluorescence signals of the second group cells incubated with LY-DCM-P were observed in the red channel, indicating the cell permeability of LY-DCM-P, and the intrinsic biothiols in HeLa cells and 4T1 cells triggered fluorescence enhancement (Figures 3B1–B6). In the third group (Figures 3C1–C6), cells were pretreated with NEM (N-ethylmaleimide, a thiol depletor), followed by incubation with LY-DCM-P for 1 h, resulting in minimal fluorescence signal detected in the red channel. In the fourth to sixth groups (Figures 3D1–F6), all cells were pre-incubated with NEM, followed by pretreatment with Cys, Hcy, and GSH, respectively. Upon the addition of LY-DCM-P, these three groups exhibited strong fluorescence signals in the red channel, which can be visually confirmed through the relative fluorescence intensity (Figures 3G and 3H).

To identify the lysosome-targeting ability of the probe LY-DCM-P, commercial lysosome-targeting dye (Lyso-Tracker Green) was further utilized for fluorescence colocalization experiments on HeLa cells and 4T1 cells. As shown in Figure 4, there was a good overlap between the fluorescence signals of the probe LY-DCM-P and the green localization dye in both HeLa

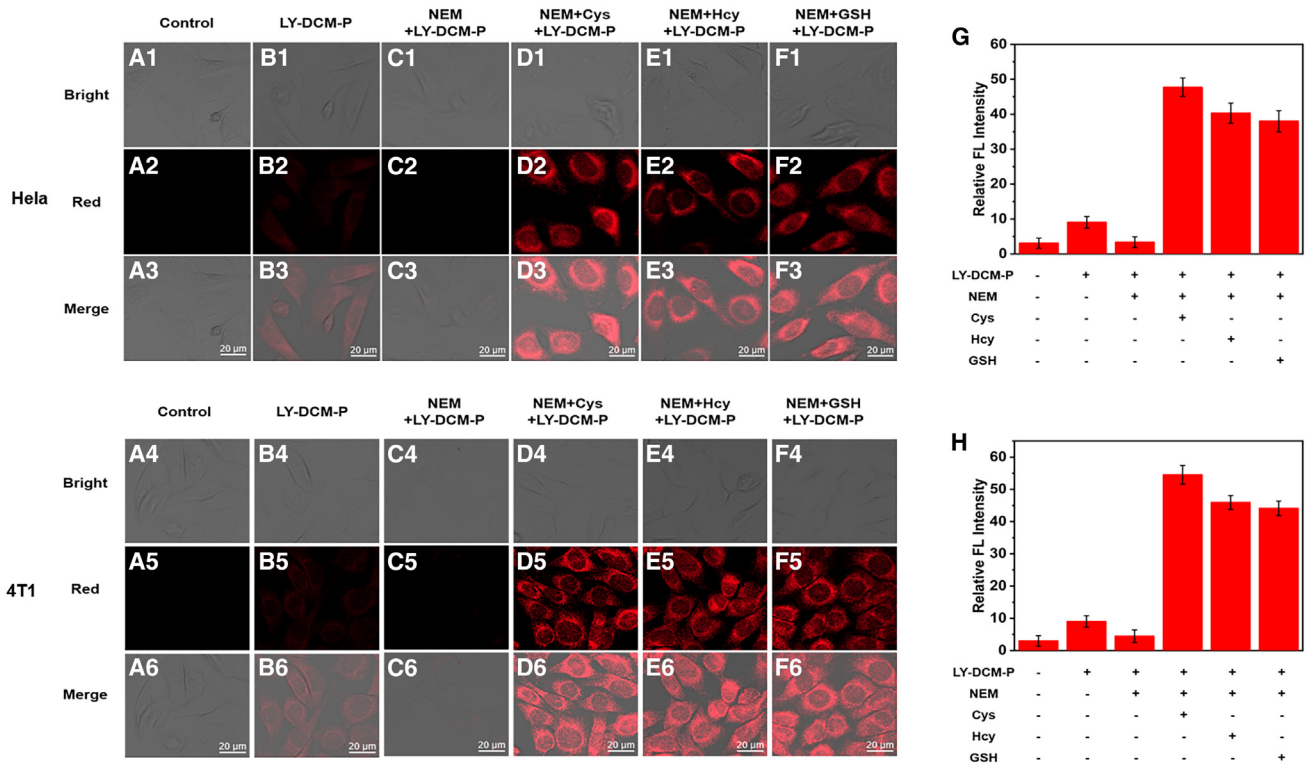

Figure 3. Fluorescence confocal imaging of probe LY-DCM-P in HeLa and 4T1 Cells

(A and B) (A) control and (B) cells were incubated with LY-DCM-P (10 μM) for 1 h.

(C) Cells were treated with NEM (200 μM) for 30 min, and then incubated with the probe (10 μM) for 1 h.

(D–F) Cells were treated with NEM (200 μM) for 30 min, followed by incubation with Cys/Hcy/GSH (200 μM) for 30 min, after which incubated with 10 μM LY-DCM-P for 1 h.

(G and H) Relative fluorescence intensity in the red channel. The error bar represents the standard deviation (n = 3), λ_{ex} = 561 nm.

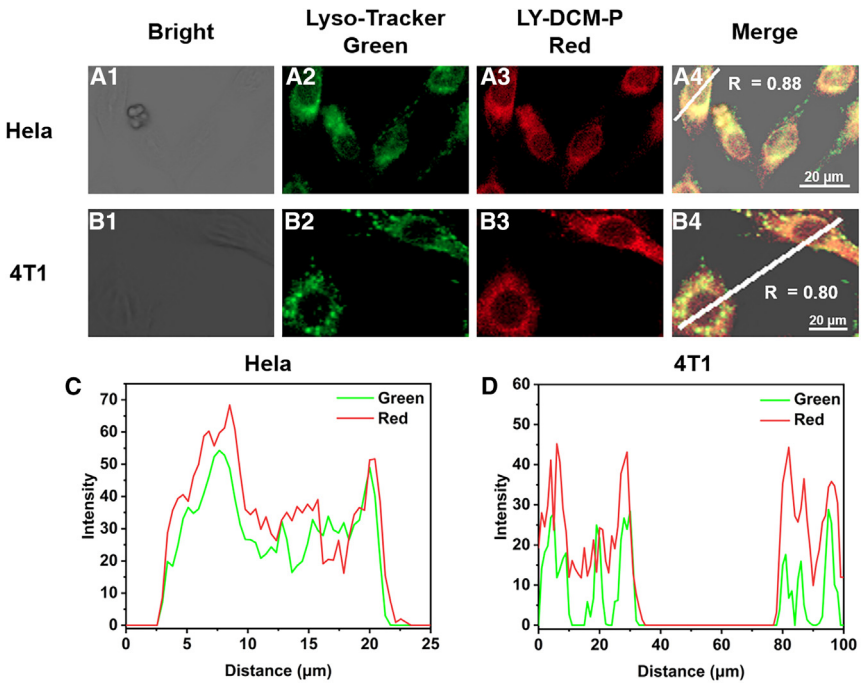

Figure 4. Imaging of subcellular co-localization of probe LY-DCM-P in HeLa cells and 4T1 cells

(A and B) HeLa cells and 4T1 cells were pretreated with Lyso-Tracker green (10 μM) for 20 min respectively, then treated with LY-DCM-P (10 μM) for 1 h, and finally imaged.

(C and D) Intensity/distance plots, data were collected from merged images of Figures 4A4 and 4B4.

cells and 4T1 cells, with Pearson coefficients of 0.88 and 0.80 (Figure 4A4 and 4B4), respectively, indicating that the probe LY-DCM-P can achieve biothiol localization at a subcellular level via fluorescence analysis.

Zebrafish imaging

The initial inspiration from cell experiments led us to validate the probe's ability of imaging biothiols *in vivo* using zebrafish, which express high levels of biogenic thiols during the embryonic stage. As shown in the Figure 5, the fluorescence emitted by zebrafish larvae in the control group can be considered negligible (Figure 5A). However, upon treatment with LY-DCM-P, fluorescence appeared in the red channel due to the presence of endogenous biogenic thiols (Figure 5B). Furthermore, when zebrafish were pretreated with NEM and then incubated with LY-DCM-P, the fluorescence was significantly inhibited (Figure 5C), indicating the tissue-penetrating property of LY-DCM-P. Similarly, subsequent treatment of zebrafish with NEM, LY-DCM-P, and endogenic biothiols resulted in a strong fluorescence signal in the red channel (Figures 5D–5F), indicating the detection of endogenous biogenic thiols in the zebrafish model.

Mice imaging

Subsequently, we were intrigued by the fluorescent imaging of biogenic thiol activity in mice (Figure 6). To investigate whether the probe LY-DCM-P could be used to detect dynamic changes in biogenic thiols *in vivo*, we implanted 4T1 cancer cells into a group of 5-week-old nude mice to establish a tumor mouse model. The tumor mice were then intratumorally injected with the LY-DCM-P probe, and fluorescence changes were observed at different time points. As shown in the figures, after injecting LY-DCM-P into the tumor mice, an obvious fluorescence signal was observed at the tumor site after 30 min, significantly enhanced after 60 min, and decreased after 90 min, indicating that LY-DCM-P has the capability to image endogenous biothiols in tumors.

Conclusions

In summary, we have designed and synthesized a lysosome-targeted fluorescent probe, LY-DCM-P, which can be used for rapid and highly selective detection of biological thiols both *in vitro* and *in vivo*. This probe exhibits long-wavelength fluorescence emission (670 nm) and a significant Stokes shift (150 nm) upon binding to biological thiols. Cell experiments have demonstrated that the probe has low cytotoxicity and excellent lysosome-targeting capability. Also, LY-DCM-P shows its advantages for imaging biological thiols in living cancer cells, zebrafish larvae, and mice. We anticipate that our contribution will offer an alternative method for studying biological thiols in living organisms and will aid in clinical research on thiol-related diseases.

Limitations of the study

Our research has certain limitations to a certain extent. The disadvantage is mainly reflected in that the probe emission wavelength is not long enough, which will affect the tissue penetration. Also, this probe has only one response factor and tumor targeting is a possible problem. For our follow-up work related to this topic, there is potential for further improvement in tumor targeting and fluorescence emission wavelengths.

RESOURCE AVAILABILITY

Lead contact

Further information and requests for resources should be directed to and will be fulfilled by the lead contact, Erfei Wang (efwang@hubu.edu.cn).

Materials availability

All unique reagents generated in this study are available from the lead contact with a completed materials transfer agreement.

Data and code availability

- The data reported in this paper will be shared by the lead contact upon request.
- This paper does not report original code.

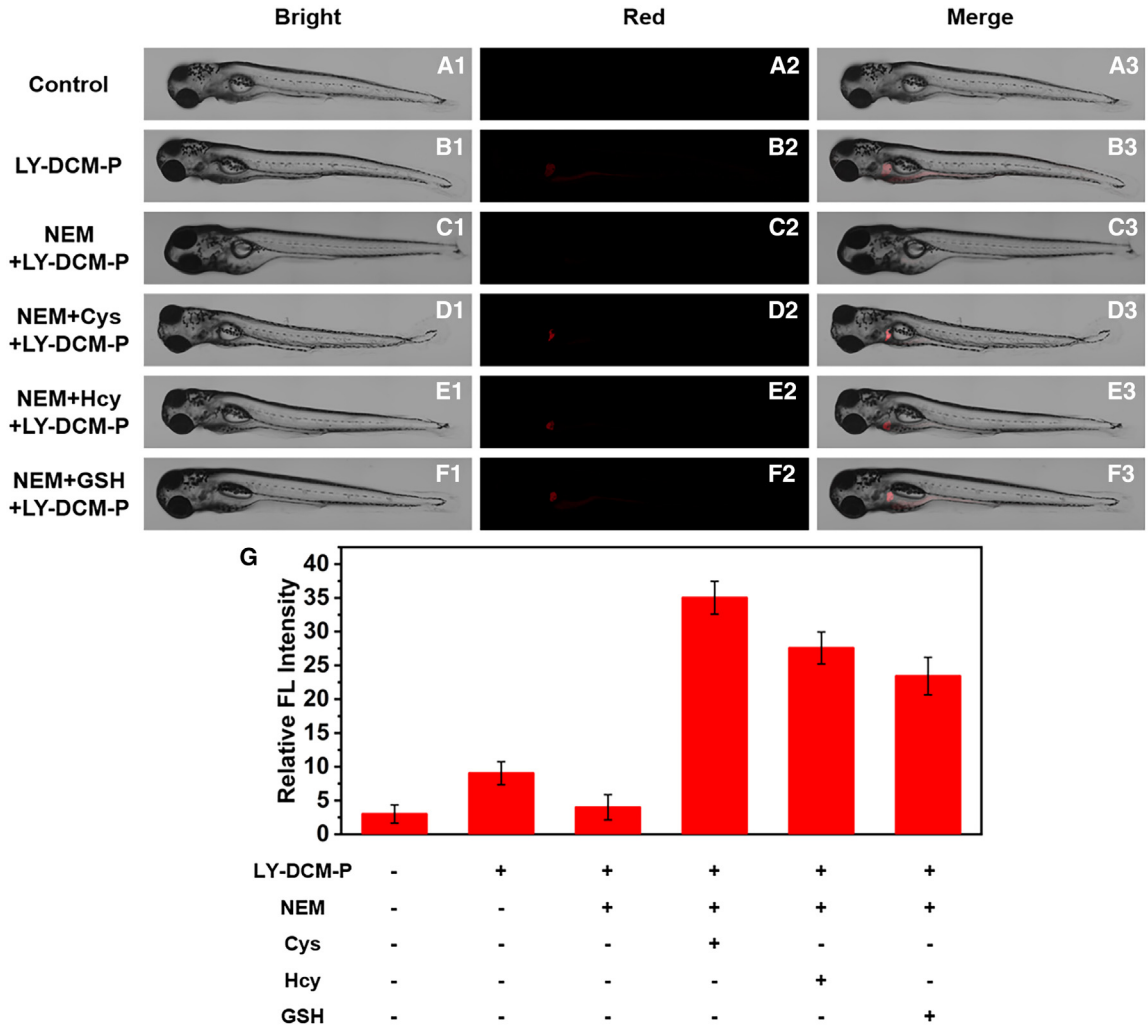

Figure 5. Fluorescence confocal imaging of probe LY-DCM-P in zebrafish

(A and B) (A) control and (B) zebrafish larvae were incubated with LY-DCM-P (10 μM) for 1 h.

(C) Zebrafish larvae were treated with NEM (200 μM) for 30 min, and then incubated with the probe (10 μM) for 1 h.

(D–F) Zebrafish larvae were treated with NEM (200 μM) for 30 min, followed by incubation with Cys/Hcy/GSH (200 μM) for 30 min, after which incubated with 10 μM LY-DCM-P for 1 h.

(G) Relative fluorescence intensity in the red channel. The error bar represents the standard deviation (n = 3), λ_{ex} = 561 nm.

- Any additional information required to reanalyze the data reported in this paper is available from the lead contact upon request.

ACKNOWLEDGMENTS

This research was financially supported by National Natural Science Foundation of China (22408091, 22278117, and 22178088), and Hubei Provincial Natural Science Foundation of China (2023AFB278).

AUTHOR CONTRIBUTIONS

T. Zhao and J.R. conceived the idea and designed the experiments. T. Zhang and Z.T. synthesized and characterized all the materials. T. Zhao and T. Zhang conducted the *in vitro* tests. X.X. and Z.Z. performed the *in vivo* fluorescence imaging tests. T. Zhao, Z.W., and E.W. wrote the manuscript. All the authors discussed the results and commented on the manuscript. J.R. supervised the overall research.

DECLARATION OF INTERESTS

The authors declare no competing interests.

STAR★METHODS

Detailed methods are provided in the online version of this paper and include the following:

- KEY RESOURCES TABLE
- EXPERIMENTAL MODEL AND STUDY PARTICIPANT DETAILS
  - Cell line
  - Animal model
- METHOD DETAILS
  - Materials and instruments
  - Synthesis of probe LY-DCM-P
  - Spectra measurement

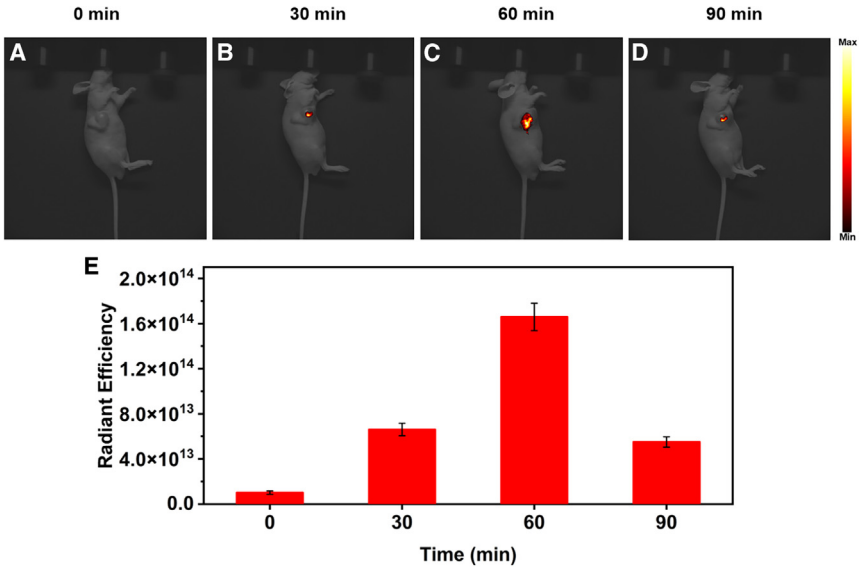

Figure 6. Fluorescence imaging of probe LY-DCM-P in mice

(A–D) Fluorescence imaging of the tumor-bearing mice after intratumoral injection of LY-DCM-P (10 μM) with time (0, 30, 60, and 90 min).

(E) Radiant efficiency in (A–D). λ_{ex} = 530 nm, λ_{em} = 600–640 nm. The error bar represents the standard deviation (n = 3).

- Selectivity assessment
- Cells culture and imaging
- Zebrafish culture and imaging
- Mice culture and imaging

- QUANTIFICATION AND STATISTICAL ANALYSIS
- ADDITIONAL RESOURCES

SUPPLEMENTAL INFORMATION

Supplemental information can be found online at https://doi.org/10.1016/j.isci.2024.111334.

Received: August 15, 2024
Revised: September 18, 2024
Accepted: November 4, 2024
Published: November 7, 2024

REFERENCES

1. Yue, Y., Huo, F., and Yin, C. (2020). The chronological evolution of small organic molecular fluorescent probes for thiols. Chem. Sci. *12*, 1220–1226. https://doi.org/10.1039/D0SC04960C.

2. Yin, C.-X., Xiong, K.-M., Huo, F.-J., Salamanca, J.C., and Strongin, R.M. (2017). Fluorescent Probes with Multiple Binding Sites for the Discrimination of Cys, Hcy, and GSH. Angew. Chem. Int. Ed. *56*, 13188–13198. https://doi.org/10.1002/anie.201704084.

3. Xue, H., Yu, M., He, K., Liu, Y., Cao, Y., Shui, Y., Li, J., Farooq, M., and Wang, L. (2020). A novel colorimetric and fluorometric probe for biothiols based on MnO2 NFs-Rhodamine B system. Anal. Chim. Acta *1127*, 39–48. https://doi.org/10.1016/j.aca.2020.06.039.

4. Zhang, J., Wang, N., Ji, X., Tao, Y., Wang, J., and Zhao, W. (2020). BODIPY-Based Fluorescent Probes for Biothiols. Chem. A Europ. J. *26*, 4172–4192. https://doi.org/10.1002/chem.201904470.

5. Kleinman, W.A., and Richie, J.P. (2000). Status of glutathione and other thiols and disulfides in human plasma. Biochem. Pharmacol. *60*, 19–29. https://doi.org/10.1016/S0006-2952(00)00293-8.

6. Liu, Y., Teng, L., Chen, L., Ma, H., Liu, H.-W., and Zhang, X.-B. (2018). Engineering of a near-infrared fluorescent probe for real-time simultaneous visualization of intracellular hypoxia and induced mitophagy. Chem. Sci. *9*, 5347–5353. https://doi.org/10.1039/C8SC01684D.

7. Bhattacharjee, P., Chatterjee, S., Achari, A., Saha, A., Nandi, D., Acharya, C., Chatterjee, K., Ghosh, S., Swarnakar, S., and Jaisankar, P. (2020). A bis-indole/carbazole based C5-curcuminoid fluorescent probe with large Stokes shift for selective detection of biothiols and application to live cell imaging. Analyst *145*, 1184–1189. https://doi.org/10.1039/C9AN02190F.

8. Sheng, H., Hu, Y., Zhou, Y., Fan, S., Cao, Y., Zhao, X., and Yang, W. (2019). A highly selective ESIPT-based fluorescent probe with a large Stokes shift for the turn-on detection of cysteine and its application in living cells. Dyes Pigm. *160*, 48–57. https://doi.org/10.1016/j.dyepig.2018.07.036.

9. Wu, Q., Wu, Y., Yu, C., Wang, Z., Hao, E., and Jiao, L. (2017). A highly selective visible light excitable boron dipyrromethene probe for cysteine over homocysteine and glutathione based on a Michael addition reaction. Sens. Actuators, B *253*, 1079–1086. https://doi.org/10.1016/j.snb.2017.07.028.

10. Ma, B., Zeng, F., Li, X., and Wu, S. (2012). A facile approach for sensitive, reversible and ratiometric detection of biothiols based on thymine-mediated excimer–monomer transformation. Chem. Commun. *48*, 6007–6009. https://doi.org/10.1039/C2CC32064A.

11. Yue, Y., Huo, F., Li, X., Wen, Y., Yi, T., Salamanca, J., Escobedo, J.O., Strongin, R.M., and Yin, C. (2017). pH-Dependent Fluorescent Probe That Can Be Tuned for Cysteine or Homocysteine. Org. Lett. *19*, 82–85. https://doi.org/10.1021/acs.orglett.6b03357.

12. Azevedo, R.S.S., de Sousa, J.R., Araujo, M.T.F., Martins Filho, A.J., de Alcantara, B.N., Araujo, F.M.C., Queiroz, M.G.L., Cruz, A.C.R., Vasconcelos, B.H.B., Chiang, J.O., et al. (2018). In situ immune response and mechanisms of cell damage in central nervous system of fatal cases microcephaly by Zika virus. Sci. Rep. *8*, 1. https://doi.org/10.1038/s41598-017-17765-5.

13. van Wijngaarden, J.P., Swart, K.M.A., Enneman, A.W., Dhonukshe-Rutten, R.A.M., van Dijk, S.C., Ham, A.C., Brouwer-Brolsma, E.M., van der Zwaluw, N.L., Sohl, E., van Meurs, J.B.J., et al. (2014). Effect of daily vitamin B-12 and folic acid supplementation on fracture incidence in elderly individuals with an elevated plasma homocysteine concentration: B-PROOF, a randomized controlled trial12345. Am. J. Clin. Nutr. *100*, 1578–1586. https://doi.org/10.3945/ajcn.114.090043.

14. Zhang, Y., Zhang, W., Chen, K., Yang, Q., Hu, N., Suo, Y., and Wang, J. (2018). Highly sensitive and selective colorimetric detection of glutathione via enhanced Fenton-like reaction of magnetic metal organic framework. Sens. Actuators, B *262*, 95–101. https://doi.org/10.1016/j.snb.2018.01.221.

15. Xu, Z., Huang, X., Han, X., Wu, D., Zhang, B., Tan, Y., Cao, M., Liu, S.H., Yin, J., and Yoon, J. (2018). A Visible and Near-Infrared, Dual-Channel Fluorescence-On Probe for Selectively Tracking Mitochondrial Glutathione. Chem *4*, 1609–1628. https://doi.org/10.1016/j.chempr.2018.04.003.

16. Zhang, H., Xia, X., Zhao, H., Zhang, G.-N., Jiang, D.-Y., Xue, X.-Y., and Zhang, J. (2019). A near-infrared fluorescent probe based on SNAr reaction for H2S/GSH detection in living cells and zebrafish. Dyes Pigm. *163*, 183–189. https://doi.org/10.1016/j.dyepig.2018.11.050.

17. Liu, Y., Zhu, S., Gu, K., Guo, Z., Huang, X., Wang, M., Amin, H.M., Zhu, W., and Shi, P. (2017). GSH-Activated NIR Fluorescent Prodrug for Podophyllotoxin Delivery. ACS Appl. Mater. Interfaces *9*, 29496–29504. https://doi.org/10.1021/acsami.7b07091.

18. Winchester, B., Vellodi, A., and Young, E. (2000). The molecular basis of lysosomal storage diseases and their treatment. Biochem. Soc. Trans. *28*, 150–154. https://doi.org/10.1042/bst0280150.

19. Fehrenbacher, N., and Jäättelä, M. (2005). Lysosomes as Targets for Cancer Therapy. Cancer Res. *65*, 2993–2995. https://doi.org/10.1158/0008-5472.CAN-05-0476.

20. Surendran, K., Vitiello, S.P., and Pearce, D.A. (2014). Lysosome dysfunction in the pathogenesis of kidney diseases. Pediatr. Nephrol. *29*, 2253–2261. https://doi.org/10.1007/s00467-013-2652-z.

21. Tang, Y.-J., Fang, W.-L., Ren, K., Guo, X.-F., and Wang, H. (2021). A turn-on homodimer fluorescent probe based on homo-FRET for the sensing of biothiols in lysosome: a trial of a new turn-on strategy. Analyst *146*, 2974–2982. https://doi.org/10.1039/D1AN00161B.

22. Tan, H., Zou, Y., Guo, J., Chen, J., and Zhou, L. (2022). A simple lysosome-targeted fluorescent probe based on flavonoid for detection of cysteine in living cells. Spectrochim. Acta, Part A *280*, 121552. https://doi.org/10.1016/j.saa.2022.121552.

23. Gong, Y.J., Kong, Z.Z., Zhang, M.-L., Lv, M.K., and Zhang, G. (2019). A structure optimized fluorescent probe for highly sensitive monitoring drug induced lysosomal pH value changes. Talanta *203*, 1–8. https://doi.org/10.1016/j.talanta.2019.05.037.

24. Gao, Q., Zhang, W., Song, B., Zhang, R., Guo, W., and Yuan, J. (2017). Development of a Novel Lysosome-Targeted Ruthenium(II) Complex for Phosphorescence/Time-Gated Luminescence Assay of Biothiols. Anal. Chem. *89*, 4517–4524. https://doi.org/10.1021/acs.analchem.6b04925.

25. Cai, S., Liu, C., Jiao, X., Zhao, L., and Zeng, X. (2020). A lysosome-targeted near-infrared fluorescent probe for imaging endogenous cysteine (Cys) in living cells. J. Mater. Chem. B *8*, 2269–2274. https://doi.org/10.1039/C9TB02609F.

26. Hori, Y., and Kikuchi, K. (2019). Chemical Tools with Fluorescence Switches for Verifying Epigenetic Modifications. Acc. Chem. Res. *52*, 2849–2857. https://doi.org/10.1021/acs.accounts.9b00349.

27. Huang, R., Wang, B.-B., Si-Tu, X.-M., Gao, T., Wang, F.-F., He, H., Fan, X.-Y., Jiang, F.-L., and Liu, Y. (2016). A lysosome-targeted fluorescent sensor for the detection of glutathione in cells with an extremely fast response. Chem. Commun. *52*, 11579–11582. https://doi.org/10.1039/C6CC06750F.

28. Li, G., Ma, S., Tang, J., and Ye, Y. (2019). Lysosome-targeted two-photon fluorescent probes for rapid detection of H2S in live cells. New J. Chem. *43*, 1267–1274. https://doi.org/10.1039/C8NJ05419C.

29. Liang, B., Wang, B., Ma, Q., Xie, C., Li, X., and Wang, S. (2018). A lysosome-targetable turn-on fluorescent probe for the detection of thiols in living cells based on a 1,8-naphthalimide derivative. Spectrochim. Acta, Part A *192*, 67–74. https://doi.org/10.1016/j.saa.2017.10.044.

30. Li, L., Liu, Q., Cai, R., Ma, Q., Mao, G., Zhu, N., and Liu, S. (2023). A novel rhodamine-based fluorescent probe for high selectively determining cysteine in lysosomes. Microchem. J. *187*, 108449. https://doi.org/10.1016/j.microc.2023.108449.

31. Zou, Y., Duan, T., Wang, Y., Ye, Q., Li, Y., Wang, X., Liu, X., Zhou, X., Yu, F., and Liu, H. (2024). Rational design of an activatable dual-color fluorogenic probe for revealing the interaction of adenosine-5′-triphosphate and peroxynitrite in pyroptosis associated with acute kidney injury. Sens. Actuators, B *418*, 136367. https://doi.org/10.1016/j.snb.2024.136367.

32. Wu, Z., Xu, N., Zhang, D., Liu, H., Li, L., Wang, F., Ren, J., and Wang, E. (2024). A mitochondria-targeted fluorescent probe for discrimination of biothiols by dual-channel imaging in living cells and zebrafish. Spectrochim. Acta, Part A *322*, 124846. https://doi.org/10.1016/j.saa.2024.124846.

33. Li, Z., Chen, S., Huang, Y., Zhou, H., Yang, S., Zhang, H., Wang, M., Guo, H., and Yin, J. (2022). Photoswitchable AIE photosensitizer for reversible control of singlet oxygen generation in specific bacterial discrimination and photocontrolled photodynamic killing of bacteria. Chem. Eng. J. *450*, 138087. https://doi.org/10.1016/j.cej.2022.138087.

34. Li, X., Liu, X., and Li, F. (2024). Configuration of super-fast Cu2+-responsive chemosensor by attaching diaminomaleonitrile to BODIPY scaffold for high-contrast fluorescence imaging of living cells. Spectrochim. Acta, Part A *304*, 123377. https://doi.org/10.1016/j.saa.2023.123377.

35. Xu, Y., Ma, H., Su, X., He, L., Wang, E., Wang, F., and Ren, J. (2023). A near-infrared self-assembled micellar nanoprobe for highly effective detection of cysteine in vitro and in vivo. Sens. Actuators, B *382*, 133564. https://doi.org/10.1016/j.snb.2023.133564.

36. Guo, Z., Nam, S., Park, S., and Yoon, J. (2012). A highly selective ratiometric near-infrared fluorescent cyanine sensor for cysteine with remarkable shift and its application in bioimaging. Chem. Sci. *3*, 2760–2765. https://doi.org/10.1039/C2SC20540H.

37. Ge, J., Fan, L., Zhang, K., Ou, T., Li, Y., Zhang, C., Dong, C., Shuang, S., and Wong, M.S. (2018). A two-photon ratiometric fluorescent probe for effective monitoring of lysosomal pH in live cells and cancer tissues. Sens. Actuators, B *262*, 913–921. https://doi.org/10.1016/j.snb.2018.02.082.

38. Wang, J., Li, B., Zhao, W., Zhang, X., Luo, X., Corkins, M.E., Cole, S.L., Wang, C., Xiao, Y., Bi, X., et al. (2016). Two-Photon Near Infrared Fluorescent Turn-On Probe Toward Cysteine and Its Imaging Applications. ACS Sens. *1*, 882–887. https://doi.org/10.1021/acssensors.5b00271.

39. Zhang, X., He, N., Huang, Y., Yu, F., Li, B., Lv, C., and Chen, L. (2019). Mitochondria-targeting near-infrared ratiometric fluorescent probe for selective imaging of cysteine in orthotopic lung cancer mice. Sens. Actuators, B *282*, 69–77. https://doi.org/10.1016/j.snb.2018.11.056.

40. Wu, Z., Zhang, D., Ma, H., Wang, E., Wang, F., and Ren, J. (2023). Near-infrared colorimetric and ratiometric fluorescent probe for dual-channel imaging of mitochondria and cysteine in the oxidative stress model. Chem. Eng. J. *475*, 146397. https://doi.org/10.1016/j.cej.2023.146397.

41. Takao, K., Endo, S., Nagai, J., Kamauchi, H., Takemura, Y., Uesawa, Y., and Sugita, Y. (2019). 2-Styrylchromone derivatives as potent and selective monoamine oxidase B inhibitors. Bioorg. Chem. *92*, 103285. https://doi.org/10.1016/j.bioorg.2019.103285.

42. Proença, C., Albuquerque, H.M.T., Ribeiro, D., Freitas, M., Santos, C.M.M., Silva, A.M.S., and Fernandes, E. (2016). Novel chromone and xanthone derivatives: Synthesis and ROS/RNS scavenging activities. Eur. J. Med. Chem. *115*, 381–392. https://doi.org/10.1016/j.ejmech.2016.03.043.

STAR★METHODS

KEY RESOURCES TABLE

REAGENT or RESOURCE	SOURCE	IDENTIFIER
Chemicals, peptides, and recombinant proteins		
4-(2-chloroethyl)morpholine hydrochloride	tansoole	3647-69-6
3-bromo-4-hydroxybenzaldehyde	tansoole	2973-78-6
acryloyl chloride	tansoole	102-92-1
N-ethylmaleimide	tansoole	128-53-0
Lyso-Tracker green	Beyotime	#C1047S
Experimental models: cell lines		
HeLa cells	servicebio	N/A
4T1 cells	servicebio	STCC00077P
Experimental models: organisms/strains		
Five-week-old nude mouse	servicebio	N/A
Zebrafish	servicebio	N/A

EXPERIMENTAL MODEL AND STUDY PARTICIPANT DETAILS

Cell line

HeLa and 4T1 cell lines were obtained from the Servicebio (Wuhan, China) and cultured according to the provided instructions.

Animal model

Zebrafish and Five-week-old nude mice were obtained from the Servicebio (Wuhan, China). All animal procedures were performed according to the Guidelines for Care and Use of Laboratory Animals of Hubei University and approved by the Animal Ethics Committee of Hubei University.

METHOD DETAILS

Materials and instruments

Unless otherwise noted, all of the reagents and solvents used in this paper were purchased from domestic suppliers and were analytically pure without further purification.

NMR hydrogen and carbon spectra were obtained using the Bruker AV-400 NMR instrument. High-resolution mass (HRMS) spectrometry data were acquired on the Agilent 1260–6224 LC-MS TOF system using ESI (electrospray ionization). HPLC was performed using the SHIMADZU LC-16. pH values were measured with the METTLER TOLEDO FiveEasy Plus pH meter. Ultraviolet-visible (UV-Vis) absorption spectra were recorded on the SHIMADZU UV-1800 spectrophotometer. Fluorescence emission spectra were obtained using the Agilent Cary Eclipse fluorescence spectrophotometer. Results from cell and zebrafish experiments were collected using the Zeiss LSM 900 laser confocal fluorescence microscope. Mice experimental data were gathered by the VISQUE *Invivo* Smart-LF *in vivo* real-time imaging system.

Synthesis of probe LY-DCM-P

Compounds 2 and 3 were synthesized following the previous method.[41,42]

Synthesis of Compound 4: To a stirred solution of Compound 3 (4.0 g, 21 mmol, 1.0 eq) and malononitrile (2.1 g, 31.5 mmol, 1.5 eq) in acetic anhydride (50 mL) was added two or three drops of piperidine at 25°C under a nitrogen atmosphere. The resulting mixture was heated to 150°C and stirred for 8 h. Upon completion of the reaction, the reaction mixture was poured into ice water (200 mL). Saturated sodium carbonate solution was added and the pH was adjusted to neutral. The mixture was then extracted with dichloromethane (100 mL × 3). The combined organic phases were washed with a saturated brine (50 mL × 3), dried over anhydrous Na_2SO_4 and filtered. The filtrate was concentrated to the residue, which was purified by column chromatography on silica (DCM: PE = 1: 4) to afford a pale yellow solid (3.4 g), yield 68%. ^{1}H NMR (400 MHz, Chloroform-*d*) δ 8.83 (d, *J* = 9.3 Hz, 2H), 7.01 (dd, *J* = 9.3, 2.7 Hz, 2H), 6.86 (d, *J* = 2.6 Hz, 2H), 6.64 (d, *J* = 0.8 Hz, 2H), 3.93 (s, 6H), 2.40 (s, 3H).

Synthesis of Compound 5: To a solution of Compound 4 (3.0 g, 12.6 mmol, 1.0 eq) in anhydrous dichloromethane (50 mL) was quickly added aluminum chloride (16.8 g, 126 mmol, 10 eq) at 25°C. The reaction was refluxed for 12 h. Upon completion of the reaction, the reaction mixture was slowly poured into ice water (100 mL). The mixture was filtered, and the filter cake was dried and

pulped with dichloromethane (10 mL) to give a pale yellow solid (1.9 g), yield 67%. ^{1}H NMR (400 MHz, DMSO-d_6) δ 11.41 (s, 1H), 8.57 (d, J = 9.2 Hz, 1H), 7.05 (dd, J = 9.2, 2.5 Hz, 1H), 6.92 (d, J = 2.5 Hz, 1H), 6.65 (d, J = 0.8 Hz, 1H), 2.44 (s, 3H).

Synthesis of Compound 6: A mixture of Compound 5 (1.0 g, 4.4 mmol, 1.0 eq), 4-(2-chloroethyl)morpholine hydrochloride (1.2 g, 6.7 mmol, 1.5 eq), and potassium carbonate (3.1 g, 22 mmol, 5.0 eq) in acetone (50 mL) was refluxed for 12 h. Upon completion of the reaction, the mixture was filtered, and the filtrate was concentrated to the residue, which was purified by column chromatography on silica (EA: PE = 1: 2 ∼ DCM: MeOH = 50: 1) to afford a yellow solid (0.9 g), yield 60%. ^{1}H NMR (400 MHz, Chloroform-d) δ 8.82 (d, J = 9.3 Hz, 1H), 7.01 (dd, J = 9.3, 2.6 Hz, 1H), 6.87 (d, J = 2.6 Hz, 1H), 6.64 (d, J = 0.8 Hz, 1H), 4.22 (s, 2H), 3.75 (t, J = 4.7 Hz, 4H), 2.87 (s, 2H), 2.61 (s, 4H), 2.40 (s, 3H)。

Synthesis of LY-DCM-OH: To a stirred solution of Compound 6 (500 mg, 1.5 mmol, 1.0 eq) and 3-bromo-4-hydroxybenzaldehyde (450 mg, 2.2 mmol, 1.5 eq) in anhydrous ethanol (50 mL) was added two or three drops of piperidine at 25°C under a nitrogen atmosphere. The resulting mixture was refluxed for 12 h. Upon completion of the reaction, the mixture was concentrated to the residue, which was purified by column chromatography on silica (DCM: MeOH = 50: 1) to afford a dark red solid (360 mg), yield 47%. ^{1}H NMR (400 MHz, Chloroform-d) δ 8.83 (d, J = 9.3 Hz, 1H), 7.71 (d, J = 2.1 Hz, 1H), 7.48–7.40 (m, 2H), 7.07 (d, J = 8.3 Hz, 1H), 7.01 (dd, J = 9.3, 2.6 Hz, 1H), 6.95 (d, J = 2.6 Hz, 1H), 6.77 (s, 1H), 6.65 (d, J = 15.9 Hz, 1H), 4.25 (t, J = 5.6 Hz, 2H), 3.76 (t, J = 4.7 Hz, 4H), 2.88 (t, J = 5.6 Hz, 2H), 2.61 (t, J = 4.7 Hz, 4H). ^{13}C NMR (101 MHz, Chloroform-d) δ 163.89, 157.01, 154.48, 154.33, 152.52, 136.38, 131.81, 129.25, 128.95, 127.53, 118.00, 117.32, 116.99, 116.13, 115.13, 111.74, 111.31, 106.65, 102.15, 77.16, 67.02, 61.27, 57.39, 54.29. HRMS (ESI) calcd for $C_{26}H_{23}BrN_3O_4^+$: 520.0866; Found: 520.0866 [M + H]$^+$.

Synthesis of LY-DCM-P: To a stirred solution of LY-DCM-OH (100 mg, 0.19 mmol, 1.0 eq) and triethylamine (58 mg, 0.57 mmol, 3.0 eq) in anhydrous dichloromethane (10 mL) was added acryloyl chloride (26 mg, 0.29 mmol, 1.5 eq) at 0°C under a nitrogen atmosphere. The reaction mixture was warmed to 25°C for 2 h. Upon completion of the reaction, the reaction mixture was poured into 20 mL of water. The mixture was separated, and the aqueous phase was extracted with dichloromethane (10 mL × 3). The combined organic phases were washed with a saturated brine (20 mL × 3), dried over anhydrous Na_2SO_4 and filtered. The filtrate was concentrated to the residue, which was purified by column chromatography on silica (DCM: MeOH = 50: 1) to afford a yellow solid (56 mg), yield 51%. ^{1}H NMR (400 MHz, Chloroform-d) δ 8.83 (d, J = 9.2 Hz, 1H), 7.84 (d, J = 2.1 Hz, 1H), 7.54 (dd, J = 8.4, 2.1 Hz, 1H), 7.49 (d, J = 15.9 Hz, 1H), 7.27 (d, J = 8.4 Hz, 1H), 7.02 (dd, J = 9.2, 2.6 Hz, 1H), 6.99 (d, J = 2.7 Hz, 1H), 6.82 (s, 1H), 6.77 (d, J = 15.9 Hz, 1H), 6.70 (dd, J = 17.3, 1.2 Hz, 1H), 6.37 (dd, J = 17.3, 10.5 Hz, 1H), 6.11 (dd, J = 10.5, 1.1 Hz, 1H), 4.29 (s, 2H), 3.77 (s, 4H), 2.91 (s, 2H), 2.65 (s, 4H). ^{13}C NMR (101 MHz, Chloroform-d) δ 163.40, 156.39, 154.48, 152.36, 149.58, 135.65, 134.41, 133.99, 132.71, 127.70, 127.55, 127.21, 124.51, 120.44, 117.28, 117.12, 115.87, 115.36, 111.66, 107.45, 105.58, 102.14, 77.16, 66.75, 62.12, 57.33, 54.22. HRMS (ESI) calcd for $C_{29}H_{25}BrN_3O_5^+$: 574.0972; Found: 574.0967 [M + H]$^+$.

Spectra measurement

All spectra were measured at 37°C in PBS buffer solution (PBS/DMSO = 3:2, v/v, 10 mM, pH = 7.4). A stock solution of LY-DCM-P (10 mM) was prepared in DMSO and then diluted with PBS buffer solution to the desired concentration (10 μM). Cys/Hcy/GSH were dissolved in ultrapure water, and other analytes were prepared in PBS buffer solution to the concentrations required for fluorescence spectroscopy. Optical tests were performed in a quartz cuvette (optical range: 1.0 cm). The excitation wavelength was set at 520 nm and the slit widths were all 10 nm.

Selectivity assessment

To study interference, LY-DCM-P (10 mM) was incubated with various analytes (100 μM) for 10 min. Initially, stock solutions of the analytes (Apr: Aprotinin, Arg: Arginine, Sul: Sulfatase, Thr: Threonine, Tyr: Tyrosinase, Lip: Lipase, Ser: Serine, Leu: Leucine, Glu: Glutamate, $CaCl_2$, $CuCl_2$, $MgCl_2$, NH_4Cl, $NaNO_2$, $Na_2S_2O_4$, Na_2SO_4, Na_2SO_3, Na_2CO_3, NaBr, $NaHSO_3$, H_2O_2, NaClO, NaHS) were dissolved in ultrapure water to a concentration of 10 mM, and then diluted to the desired concentration with PBS buffer. The fluorescence spectra were then measured.

Cells culture and imaging

HeLa cells and 4T1 cells were cultured in Dulbecco's Modified Eagle Medium (DMEM) supplemented with 10% fetal bovine serum and 1% penicillin/streptomycin, under conditions of 37°C and 5% CO_2 humidity. For confocal imaging, HeLa cells and 4T1 cells were treated with LY-DCM-P (10 μM) for 1 h, followed by three washes with PBS prior to imaging. In the inhibitor group, cells were pretreated with NEM (200 μM) for 30 min, washed with PBS, and then incubated with LY-DCM-P (10 μM) for an additional 1 h. In the experimental group, cells were treated with NEM (200 μM) for 30 min, followed by incubation with Cys/Hcy/GSH (200 μM) for 30 min, after which 10 μM LY-DCM-P was added and the incubation continued for another 1 h. All cells were washed before im aging. Fluorescence images were captured on a Zeiss LSM 900 confocal microscope.

Zebrafish culture and imaging

Zebrafish pretreated with 1-phenyl-2-thiourea (PTU) were incubated in embryonic medium at 25°C for 3 to 7 days. Subsequently, the zebrafish were incubated with LY-DCM-P (10 μM) for 1 h. In the third group, the zebrafish were first incubated with NEM (200 μM) for 30 min, washed three times with PBS, and then LY-DCM-P (10 μM) was added for an additional 1 h incubation. In the experimental group, the zebrafish were pretreated with NEM (200 μM) for 30 min, followed by a 30-min incubation with Cys/Hcy/GSH (200 μM).

Then, LY-DCM-P (10 μM) was added and incubated for another 1 h. Prior to imaging, all samples were washed three times with PBS, and fluorescence images were acquired on a Zeiss LSM 900 confocal microscope.

Mice culture and imaging

Five-week-old nude mice with an average weight of 30 ± 2 g were subcutaneously injected with 4T1 cells and incubated for 14 days for mice imaging. LY-DCM-P (10 μM) was injected into the tumor site of the mice, and then fluorescence images were acquired at different times (0–90 min) at the excitation wavelength of 530 nm, red channel 600–640 nm.

QUANTIFICATION AND STATISTICAL ANALYSIS

This study does not involve quantification and statistics.

ADDITIONAL RESOURCES

There are no additional resources need to be declared in this manuscript, additional requests for this can be made by contacting the lead contact.